ANNALS OF GEOPHYSICS, 66, 1, DM104, 2024; doi:1044.01/ag-9042
OPEN ACCESS

Research on the Rayleigh surface wave inversion method based on the improved whale optimization algorithm

Wang Ren[1,2,3], Zhenan Yao[*,1,2,3], Zhibing Feng[1,2,3], Wenjie Li[1,2,3], Xiangteng Wang[1,2,3], Pan Wang[1,2,3], Chenhao Zhan[1,2,3]

(1) State Key Laboratory of Nuclear Resources and Environment, Nanchang, China, 330013
(2) Jiangxi Provincial Earthquake Disaster Mitigation and Engineering Geological Disaster Detection Engineering Research Center, Nanchang, China, 330013
(3) School of Geophysics and Measurement-Control Technology, East China University of Technology, Nanchang, China, 330013

Article history: received November 16, 2023; accepted January 21, 2024

Abstract

Surface wave exploration is widely used in fields such as near-surface exploration and engineering surveys because of its advantages of high resolution near the surface, non-destructive testing, convenient construction, and high-cost performance. Dispersion curve inversion is a key step in surface wave exploration, and the inversion accuracy of subsurface elastic parameters is heavily dependent on the inversion method. Similar to other geophysical inversion problems, dispersion curve inversion has inherent defects such as multiple parameters and multiple extreme values. Therefore, the use of linear methods has certain uncertainties and instability. From the perspective of global optimization nonlinearity, this paper introduces the whale optimization algorithm (WOA) and improves it. The three population update mechanisms of the WOA are independent of each other, so the global exploration and local development processes in the optimization phase can be run and controlled separately. In addition, WOA does not require the artificial setting of various control parameter values, which improves the efficiency of the algorithm and reduces the difficulty of application. However, the WOA application still has slightly lower convergence precision and result accuracy in dispersion curve inversion, so this paper also proposes an improved whale optimization algorithm (IWOA) based on WOA. IWOA optimizes the initialization of the population and adds adaptive weight coefficients to enrich the population information and improve the convergence ability and local search ability of the algorithm. To test the applicability and noise immunity of IWOA for dispersion curve inversion, the noise-free and noise-contaminated dispersion curves of three theoretical models were inverted with IWOA. IWOA was also applied to the study of multi-mode model dispersion curve inversion. At the same time, the particle swarm optimization (PSO) algorithm and WOA were also tested in the same inversion test to compare the performances of the PSO, WOA, and IWOA. The results of the above various experimental analyses show that IWOA has good applicability and noise immunity in the dispersion curve inversion of the theoretical model. The multi-mode dispersion curve inversion results show that IWOA is not only suitable for the inversion of multi-mode data but also can significantly improve the accuracy of the inversion results. Compared with PSO and WOA, IWOA has a more stable convergence process and higher convergence accuracy. Finally, the measured data from the Arnarbæli area in Iceland (fundamental-mode surface wave data)

and the Wyoming area in the United States (multi-mode surface wave data) were inverted to test the practicality of IWOA in inverting measured data. Analysis of measured data shows that IWOA is very suitable for the inversion of dispersion curves and can effectively quantitatively explain and solve practical engineering problems.

Keywords: The Rayleigh surface wave; Dispersion curve inversion; Global optimization algorithm; The whale optimization algorithm; The particle swarm optimization algorithm

1. Introduction

Since the Rayleigh surface waves were discovered by British scholar Rayleigh [1885], they have attracted widespread attention and research by many scholars. The Rayleigh waves are a type of waves formed by the interference and superposition of longitudinal and share waves and they propagate along the surface or medium interface. When the Rayleigh surface wave propagates through layered media, its phase velocity changes with variations in frequency. Subsequently, numerous scholars utilized the characteristics of Rayleigh waves in their research on near-surface geological structures. With the deepening of research, people have found that Rayleigh waves are often distributed in groups according to frequency in seismic records, and Rayleigh waves at different frequencies reflect stratigraphic information at different depths in the medium. Meanwhile, the frequency dispersion characteristics of the Rayleigh waves are affected by the longitudinal wave velocity, shear-wave velocity, thickness, and density of various layers, among which, the shear-wave velocity and thickness most affect the Rayleigh waves. Therefore, the inversion of the dispersion curve of Rayleigh waves can obtain a relatively accurate determination of shear wave velocities and thickness information for each layer of the underground medium. At present, with the rapid development of science technology and electronic information, Rayleigh wave exploration technology has been relatively mature. Because of its advantages [Wu et al., 2017] of high resolution near the surface, non-destructive testing, convenient construction, and high-cost performance, It is widely used in many fields such as roadbed assessment and evaluation [Zhu et al., 2022], landslide investigation [Zhou et al., 2008], geological hazard assessment [Zhang, 2018], coal exploration [Xu et al., 2014] and other fields.

The technical process of surface wave exploration can be roughly divided into three steps: (1) Collection of field measurement data; (2) Extraction of dispersion curves; (3) Inversion of the dispersion curves. The inversion results of the dispersion curve can obtain information on the subsurface shear wave velocity structure, and the quality of these results directly affects the accuracy and reliability of the obtained information. Therefore, dispersion curve inversion is also the most important step in the entire Rayleigh wave exploration technology. Currently, dispersion curve inversion methods can be broadly categorized into two main classes: global non-linear optimization algorithms and local linear optimization algorithms. Common local linear optimization algorithms include methods like the least-squares method [Dorman et al., 1962; Cercato, 2010], Occam's algorithm [Constable et al., 1987; Wang et al., 2009], singular value decomposition [Ding, 2004] and others, which have a high inversion speed. However, local linear optimization algorithms have high requirements for the establishment of the initial model and require high-precision derivatives. Therefore falling into the local extremum by using such methods is easy. Common global nonlinear optimization algorithms include particle swarm optimization (PSO) [Song et al. 2012; Cai et al. 2018; Zhang et al. 2016], genetic algorithm (GA) [Shi et al. 1995; Lei et al. 2019; Ni et al. 2018], simulated annealing algorithm (SA) [Ryden et al. 2006; Calderon et al. 2007; Beaty et al. 2002], sparrow search algorithm (SSA) [Sun et al. 2022], among others. This type of algorithm has minimal dependence on the established initial models, high solution accuracy, and strong capability to jump out of the local optimal solution. However, when dealing with complex subsurface structures, global nonlinear optimization algorithms will have problems of slow convergence speed and low convergence accuracy.

Regarding the shortcomings of the above-mentioned global nonlinear optimization algorithm, this article introduces the Whale Optimization Algorithm (WOA) proposed by Mirjalili from Griffith University, Australia, in 2016. The three population update mechanisms of this algorithm are independent of each other, so the global exploration and local development processes in the optimization phase can be run and controlled separately.

In addition, this algorithm does not require the artificial setting of various control parameter values, which improves the efficiency of the algorithm and reduces the difficulty of application. Compared with other swarm intelligence optimization algorithms such as PSO, SSA, etc., the WOA has a novel structure and fewer control parameters. Therefore, this algorithm shows very good optimization performance in solving many numerical optimization and engineering problems [Mirjalili et al., 2016; Bui et al., 2021]. By making improvements based on this algorithm in this paper, an Improved Whale Optimization Algorithm (IWOA) was proposed and applied to the inversion research of the Rayleigh wave dispersion curve. IWOA adopts two optimization strategies: sin chaotic population initialization and adding adaptive weight coefficient ω. The above two strategies make the distribution of the initial population more uniform, enhance individual search capabilities, and improve the convergence accuracy of the algorithm.

In this article, to assess the convergence capabilities of IWOA, two multimodal complex mathematical functions were used to test the algorithm. Three typical theoretical geological models were established, and both noise-contaminated and noise-free dispersion curves were used to test the inversion accuracy and anti-noise ability of IWOA. Additionally, This paper applied IWOA to the dispersion curve inversion of multi-mode of the theoretical model to verify whether IWOA can invert the dispersion curves of multi-mode. Then, to compare the performance of IWOA with other algorithms, IWOA was applied to the same models for comparative analysis experiments with WOA and PSO. Finally, IWOA was used to invert the measured data from two different regions to test the algorithm's ability to invert actual data. The results of the theoretical model and measured data analysis show that IWOA has the characteristics of stability, high accuracy, and strong applicability, and can effectively quantitatively explain Rayleigh wave dispersion curves.

2. The whale optimization algorithm

2.1 Method principle

The WOA is a new swarm intelligence optimization algorithm proposed by Mirjalili [2016], a scholar from Griffith University in Australia, 2016. Whales are special animals and are considered the largest mammals in the world. At the same time, relevant research has proven that whales can think, learn, and judge like humans. Another difference is in the whales' social behavior. Whales usually live together in groups and hunt together. The way whales hunt is also different from that of other animals. They create unique bubbles along a circular or '9'-shaped path (as shown in Figure 1) and move from the deep sea to the shallow water to feed on swarms of krill and small fish. The WOA

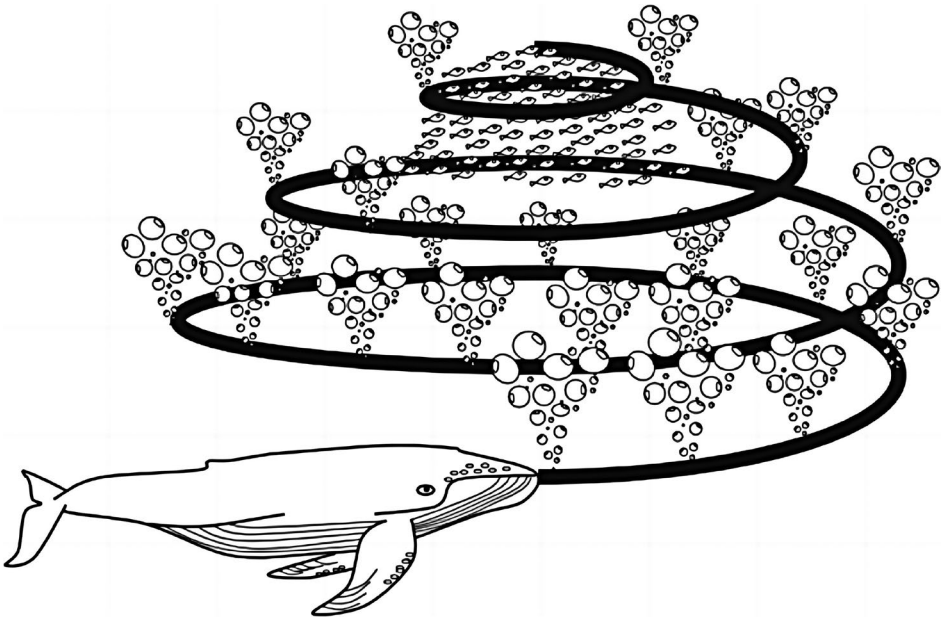

Figure 1. Bubble-net feed behavior of whales [Mirjalili et al. 2016].

simulates the hunting process of a humpback whale from discovery to prey capture. This process corresponds to three stages of the algorithm: surrounding prey, hunting behavior, and searching for prey.

The mathematical steps of the WOA are described below:

(1) Population individual position initialization.

$$X_i^t = X_{low} + rand \times \left(X_{up} - X_{low}\right); \quad i = 1,2,3 \ldots N; \quad t = 1,2,3 \ldots T \tag{1}$$

Where X_i^t represents the position of the i^{th} individual when the current iteration number is t, X_{up} and X_{low} represent the upper and lower bounds of the search space respectively, N represents the number of populations, T represents the maximum number of iterations, and $rand$ represents a random number between 0 and 1.

(2) Surrounding prey stage.

The whale population first seeks the area where the prey is located. With an increase in the number of iterations, whales will progressively approach the prey, and their positions will continuously update. If the current location of the prey is the best position for the whale population, the other whales will move towards this optimal position to complete the hunting of the prey. The formula for updating the positions of individual whales in the population is as follows:

$$X_i^{t+1} = X_b^t - A \times D_1 \tag{2}$$

$$D_1 = \left|C \times X_b^t - X_i^t\right| \tag{3}$$

$$A = 2a \times rand - a \tag{4}$$

$$C = 2rand \tag{5}$$

$$a = 2 - 2t/T \tag{6}$$

Where X_i^{t+1} represents the position of the i^{th} individual when the current iteration number is $t+1$, X_b^t represents the optimal position of the individual when the iteration number is t, D_1 represents the step length to surround the prey, A and C represent the variable coefficients, and a represents the convergence factor.

(3) Hunting behavior stage.

According to the unique hunting behavior of whales, which involves moving towards the prey in a spiral trajectory. As the number of iterations increases, the whales' encirclement radius continuously narrows to facilitate better prey capture. During the spiral movement of whales, the formula for updating the spiral position is as follows:

$$X_i^{t+1} = X_b^t + D_2 \times e^{ZM} \times \cos(2\pi M) \tag{7}$$

$$D_2 = \left|X_b^t - X_i^t\right| \tag{8}$$

Where D_2 represents the distance between the individual whale and the prey, Z represents the factor that determines the shape of the spiral, and M represents a random number between -1 and 1. However, in actual hunting, contraction

encirclement mode and spiral motion mode are carried out simultaneously 0, and each of the two hunting modes accounts for half. The mathematical formula is expressed as

$$X_i^{t+1} = \begin{cases} X_b^t - A \times D_1 & if\ p < 0.5 \\ X_b^t + D_2 \times e^{ZM} \times \cos(2\pi M) & if\ p \geq 0.5 \end{cases} \tag{9}$$

(4) Searching prey stage.

To increase the hunting range, whales also adopt a random movement pattern for hunting. This pattern does not depend on prey to update individual positions but relies on global random searches among the positions of whale individuals to select new positions. The mathematical formula for updating positions in this random movement pattern is as follows:

$$X_i^{t+1} = X_{rand}^t - A \times D_3 \tag{10}$$

$$D_3 = \left| C \times X_{rand}^t - X_i^t \right| \tag{11}$$

Where X_{rand}^t represents the random position of the individual whale, and D_3 represents the distance between the selected random position and the prey position.

The pseudo-code of the WOA algorithm is presented in Table 1.

Input: Maximum number of iterations T and whales population N
Initialize the position of the individual whale by Eq. (1)
Calculate the fitness value of each whale population f_i
F_{best} *= the best position for hunting*
while *(t<T)*
  for *every individual*
    Update parameters A, C, a, P, and M in Eq. (2), Eq. (10), and Eq. (7)
    if *(p<0.5)*
      if *(|A|<1)*
        Update the position of the current individual by Eq. (2)
        $X_i^{t+1} = X_b^t - A \times D_1$
      else if
        Select a random individual X_{rand}^t
        Update the position of the current individual by Eq. (10)
        $X_i^{t+1} = X_{rand}^t - A \times D_3$
      end if
    else if *(p≥0.5)*
        Update the position of the current individual by Eq. (7)
        $X_i^{t+1} = X_b^t + D_1 \times e^{ZM} \times \cos(2\pi M)$
    end if
  end for
  Boundary processing and Calculate the fitness value of each whale population f_i
  Update F_{best} *(if there is a better solution)*
  t = t+1
end while
Return F_{best}

Table 1. Pseudo-code of the WOA algorithm.

2.2 Improvement strategies

2.2.1 Sin chaos population initialization

The quality of the initialized population has a significant impact on the performance of the algorithm, so the initialization of the population is particularly critical. The WOA uses a random method to initialize the population, which will lead to high randomness, poor diversity, and individual aggregation within the population, resulting in uneven population distribution in the search space. To address the above problems, this paper adopts the Sin chaotic initialization strategy [Yang et al., 2009] in the population initialization process of WOA. Sin chaotic population initialization ensures an even distribution of the population in the search space and increases the diversity of population information. To a certain extent, this strategy can improve the algorithm's ability to jump out of the local optimal solution and the accuracy of the algorithm results. The one-dimensional mapping mathematical formula of Sin chaotic initialization is as follows:

$$\begin{cases} X_{n+1} = \sin(2/x_n) & n = 0,1,\dots N \\ -1 \le x_n \le 1 & x_n \neq 0 \end{cases} \tag{12}$$

Where X_{n+1} and x_n represent the positions of the $n+1^{\text{th}}$ and n^{th} individuals respectively. $x_n \neq 0$ is to prevent the creation of zero points and constant points.

2.2.2 Adding adaptive weight coefficient ω

The traditional WOA performs well in searching for the optimal location early, and it does not depend on information from other individuals. However, in the later stage of the algorithm, the population easily falls into the local optimal area, leading to problems of unstable and incomplete convergence. To address these problems, this paper introduces a non-linearly decreasing weight coefficient ω [Zhang et al., 2023], which decreases non-linearly as the number of iterations increases. In the early stage of the algorithm, when the number of iterations is small, the weight coefficient ω will be larger, allowing the algorithm to quickly approach the vicinity of the optimal position. At this point, the population also has good global search capabilities. In the later stage of the algorithm, when the number of iterations is high, the weight coefficient ω will be small, enabling the algorithm to perform a more detailed and slower search in the vicinity of the optimal position. At this time, the population gradually converges towards the global optimal position, improving the algorithm's convergence and local search capabilities. The population position updating formula with the adaptive weight coefficient ω and the calculation formula for the adaptive weight coefficient ω are as follows:

$$X_i^{t+1} = \omega \times X_b^t - A \times D_1 \tag{13}$$

$$X_i^{t+1} = \omega \times X_b^t + D_2 \times e^{ZM} \times \cos(2\pi M) \tag{14}$$

$$\omega = \omega_{max} + (\omega_{max} - \omega_{min}) \times 2/\pi \times \arccos(t/T) \tag{15}$$

Where ω_{max} and ω_{min} represent the maximum and minimum values of the weight coefficient respectively. After verification, the algorithm has the best optimization ability when the maximum and minimum values are 0.8 and 0.3 respectively. t represents the current number of iterations, and T represents the maximum number of iterations.

The IWOA flow chart is shown in Figure 2.

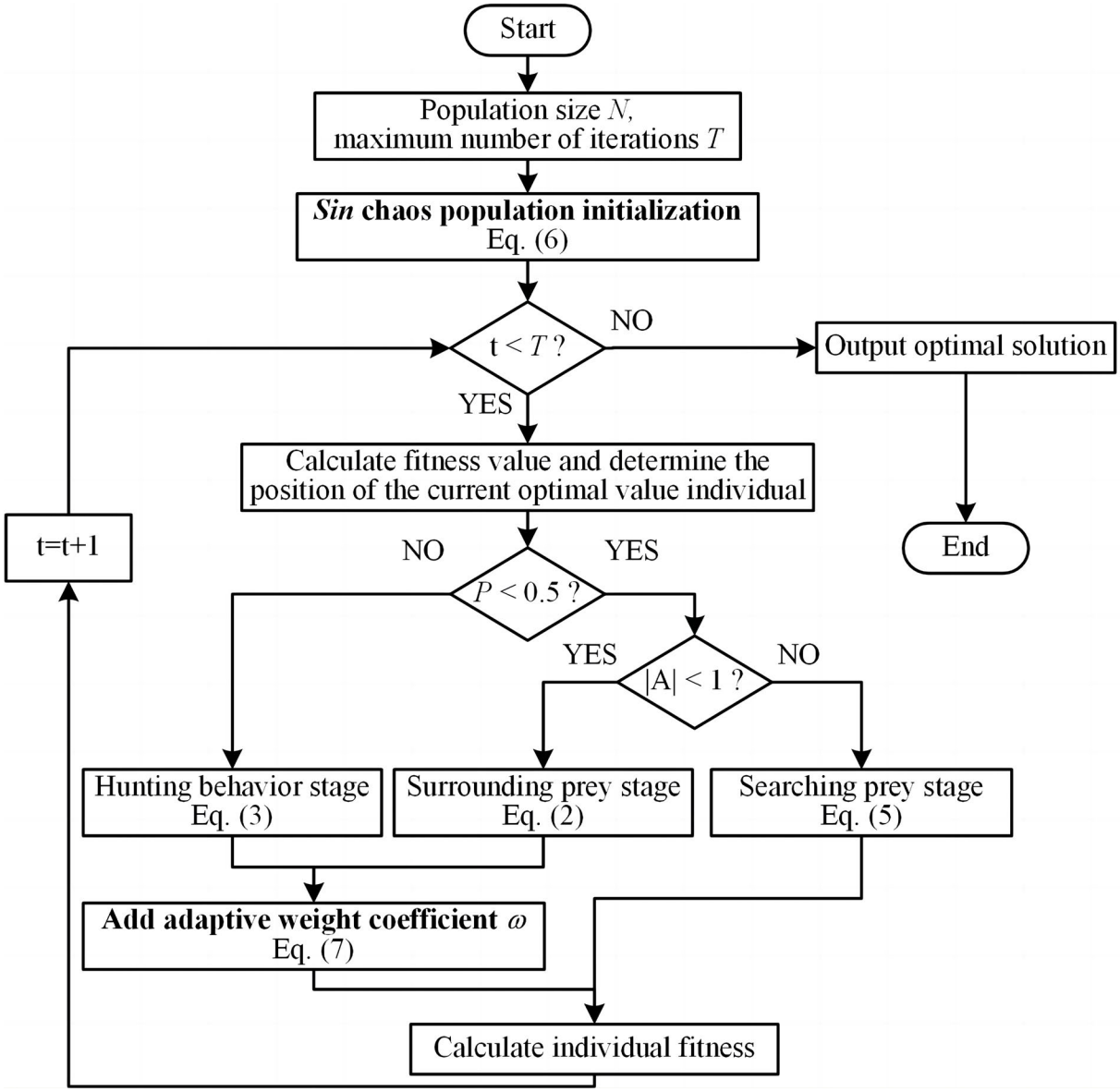

Figure 2. IWOA algorithm flowchart.

2.3 Algorithm testing

This paper selects two complex multimodal functions for algorithm testing to verify the performance of IWOA in dealing with complex problems. The function F_1 is a quartic function containing random noise with many local minima distributed within its search range, so this function can be a good test of the search capability of the algorithm. The function F_2 is a complex nonlinear function with a broad search space and can test the convergence ability of the algorithm. The above two functions are generally considered to be complex multi-modal problems that are difficult to handle by many optimization algorithms. Therefore, the above two functions are selected in this paper to test the performance of the IWOA algorithm. The mathematical expressions of the two functions are as follows:

$$\begin{cases} F_1(x) = \sum_{i=1}^{2} i x_i^4 + random[0,1) & -1 \le x_i \le 1 \\ F_2(y) = 20 + e - 20 \times e^{-0.2(0.5\sum_{i=1}^{2} y_i^2)^{0.5}} - e^{0.5\sum_{i=1}^{2}\cos 2\pi y_i} & -20 \le y_i \le 20 \end{cases} \tag{16}$$

The figures of the above two functions are shown in Figure 3. From the figure, it can be observed that the global minimum values of the two functions are both 0, and both are located at (0, 0). In this paper, IWOA and WOA are

applied to find the global minimum values for these two functions. The population number was set to 30, and the number of iterations was set to 100 for each test. The average results from 10 times are reported as the final results. The calculated results and error analysis are presented in Table 2.

Based on the results in Table 2, it can be seen that both IWOA and WOA perform well in finding the global minimum values on the two complex multimodal functions. However, IWOA's results are significantly better than WOA's in terms of mean, standard deviation, and optimal solution. Through the above comparison, the results show that IWOA enhances search capabilities and improves solution accuracy based on WOA. IWOA has strong optimization abilities and the capability to converge toward optimal solutions, especially when dealing with complex problems.

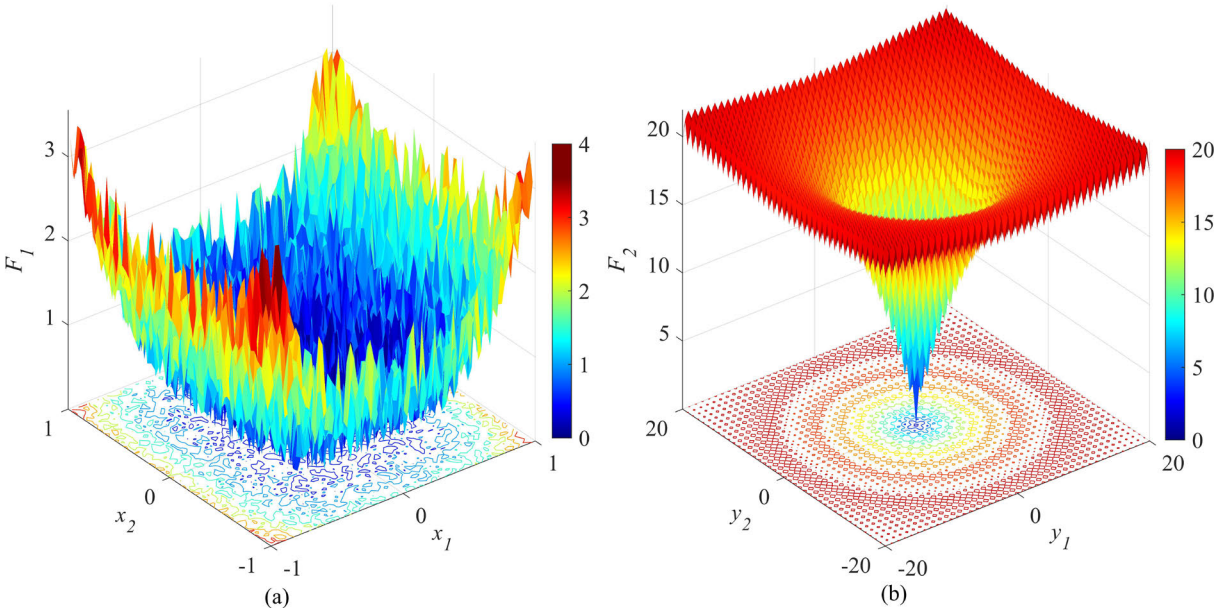

Figure 3. Image of F_1 function (a) and F_2 function (b).

Test function	True value	WOA			IWOA		
		Optimal solution	Mean	Standard deviation	Optimal solution	Mean	Standard deviation
F_1	0	5.54×10^{-4}	1.99×10^{-2}	1.3×10^{-2}	5.22×10^{-5}	6.18×10^{-3}	7×10^{-3}
F_2	0	9.12×10^{-9}	4.03×10^{-7}	5.27×10^{-7}	7.99×10^{-15}	3.18×10^{-7}	9.88×10^{-6}
Note: All numbers must have 2 significant digits after the decimal point.							

Table 2. Optimization results and error analysis of WOA and IWOA.

2.4 Parameter and objective function settings

Based on previous research, the two primary parameters that significantly affect the inversion of dispersion curves are shear wave velocity and layer thickness, and other parameters like density and Poisson's ratio have minimal impact on the dispersion curves [Xia, 2014]. To save computational resources, this paper focuses on inverting shear wave velocity and layer thickness, and all the other parameters are set to known values. Considering that the estimated values of compressional wave velocity and density may have some deviations from the true values in practical work, the search ranges for these parameters were set to be 50% of the true model values during inversion. In the subsequent inversion of the theoretical model and measured data, the population number was set to 20, and the number of iterations was set to 20. To reduce the random influence caused by a single inversion result, the number of inversions is set to 20, and the average of the 20 inversion results is used as the final result.

The inversion problem of the Rayleigh waves dispersion curves is fundamentally a problem of finding the minimum value of an objective function. When various parameters in the subsurface medium, such as layer thickness, density, shear and longitudinal wave velocities, and frequency, are provided, we can calculate the phase velocity of the Rayleigh waves based on these parameters. However, during the inversion process, the shear wave velocity and layer thickness are no longer given definite values but a range of values. The values of other parameters remain constant, and random values within the given parameter ranges are chosen. Subsequently, the phase velocity of the inverted Rayleigh waves can be calculated. Finally, the phase velocity before and after the inversion is calculated using a certain functional relationship (the closer the phase velocity values before and after the inversion are, the smaller the function value will be). When the function value is smaller, it indicates that the inverted model is closer to the true model. The objective function used in this paper during the inversion is the root mean square error between the inverted velocity values and the theoretical velocity values, and its mathematical formula is as follows:

$$P_1(M) = \sqrt{\sum_{i=1}^{N} (v_i^{inversed} - v_i^{truth})^2 / N} \tag{17}$$

Where M represents the inversion model, N represents the number of frequency points of the dispersion curve, v_i^{truth} represents the Rayleigh wave velocity at the i^{th} frequency point calculated by forward modeling of model parameters, and $v_i^{inversed}$ represents the Rayleigh wave velocity at the i^{th} frequency point on the inversion dispersion curve.

For the objective function of multi-mode dispersion curve inversion, its mathematical formula is as follows:

$$P_2(M) = \left(\sum_{i=1}^{A} \sqrt{\sum_{r=1}^{N} (v_{i,r}^{inversed} - v_{i,r}^{truth})^2 / N_i} \right) \Big/ A \tag{18}$$

Where A represents the number of high-mode dispersion curves, and N_i represents the number of frequency points of the i^{th} dispersion curve. The forward simulation of the dispersion curve used in this paper is the fast scalar method [Fan et al. 2002].

3. Theoretical model inversion analysis

Three common theoretical geological models were established to test the algorithm and evaluate the effectiveness and noise immunity of the IWOA in this paper. The longitudinal wave velocity (V_P), shear wave velocity (V_S), density (ρ), layer thickness (H) parameter, the search range settings of shear wave velocity, and layer thickness are shown in Table 3. Model A is a four-layer speed incremental model, model B is a four-layer incremental model including a low-speed layer, and model C is a four-layer incremental model including a high-speed layer. The frequency range of models A and B is set to 5~100 Hz. The frequency interval is set to 3 Hz. Model C cannot observe the fundamental-mode wave when the frequency is higher than 70 Hz. Therefore, its frequency range is set to 5~70 Hz, and the frequency interval is also set to 3 Hz.

Model	Layer number	Model parameters				Search scope	
		V_S [m/s]	V_P [m/s]	ρ [g/cm^3]	H [m]	V_S [m/s]	H [m]
A	1	150	498	2.0	2	75~225	1~3
	2	200	663	2.0	2	100~300	1~3
	3	300	995	2.0	4	150~450	2~6
	4	400	1327	2.0	∞	200~600	∞
B	1	200	663	2.0	2	100~300	1~3
	2	160	473	2.0	3	80~240	1.5~4.5
	3	300	829	2.0	3	150~450	1.5~4.5
	4	400	1327	2.0	∞	200~600	∞
C	1	160	521	2.0	2	80~240	1~3
	2	250	860	2.0	3	125~375	1.5~4.5
	3	200	650	2.0	4	100~300	2.5~7.5
	4	400	1327	2.0	∞	200~600	∞

Table 3. Geological parameters and inversion search scope of models A, B, and C.

3.1 Noise-free model inversion

In the actual collected seismic data, the fundamental-mode waves have the characteristics of strong energy, easy extraction, and easy extraction. Therefore, the main focus of this paper is on the inversion of shear wave velocity for fundamental-mode waves. To validate and evaluate the applicability of the algorithm, this article first applied IWOA in the inversion of dispersion curve data of models A, B, and C without noise. The inversion results are shown in Figure 4 and Table 4.

Figures a1, b1, and c1 in Figure 4 represent the dispersion curves before and after inversion for models A, B, and C, respectively. The light blue solid lines represent the dispersion curve results for each independent inversion run (a total of 20 runs). The green solid lines represent the theoretical dispersion curves. The orange dashed lines represent the averaged dispersion curve results over the 20 runs. Figures a2, b2, and c2 in Figure 4 show the shear wave velocity structures before and after inversion for models A, B, and C, respectively. The light blue solid lines represent the shear wave velocity results for each independent inversion run (20 runs in total). The green solid lines represent the true shear wave velocity structures. The orange dashed lines represent the averaged shear wave velocity results over the 20 runs. Table 4 provides a statistical summary of the results of IWOA applied to the inversion of dispersion curves for both noise-contaminates and noise-free models A, B, and C. Table 4 includes the mean, relative error, and standard deviation results for each inversion parameter.

It can be seen from Figure 4 that the dispersion curve results by IWOA fit well with the theoretical dispersion curves for all three models. The inverted shear wave velocity structures also exhibit good agreement with the actual shear wave velocity structures, especially the best inversion results in model C. According to the results in Table 4, it can be calculated that the average relative errors of models A, B, and C are 0.71%, 1.31%, and 0.53% respectively, and the average standard deviations are 2.32, 1.56, and 0.41 respectively. These results indicate that IWOA has excellent applicability in the inversion process and can accurately and effectively invert the Rayleigh wave dispersion curve.

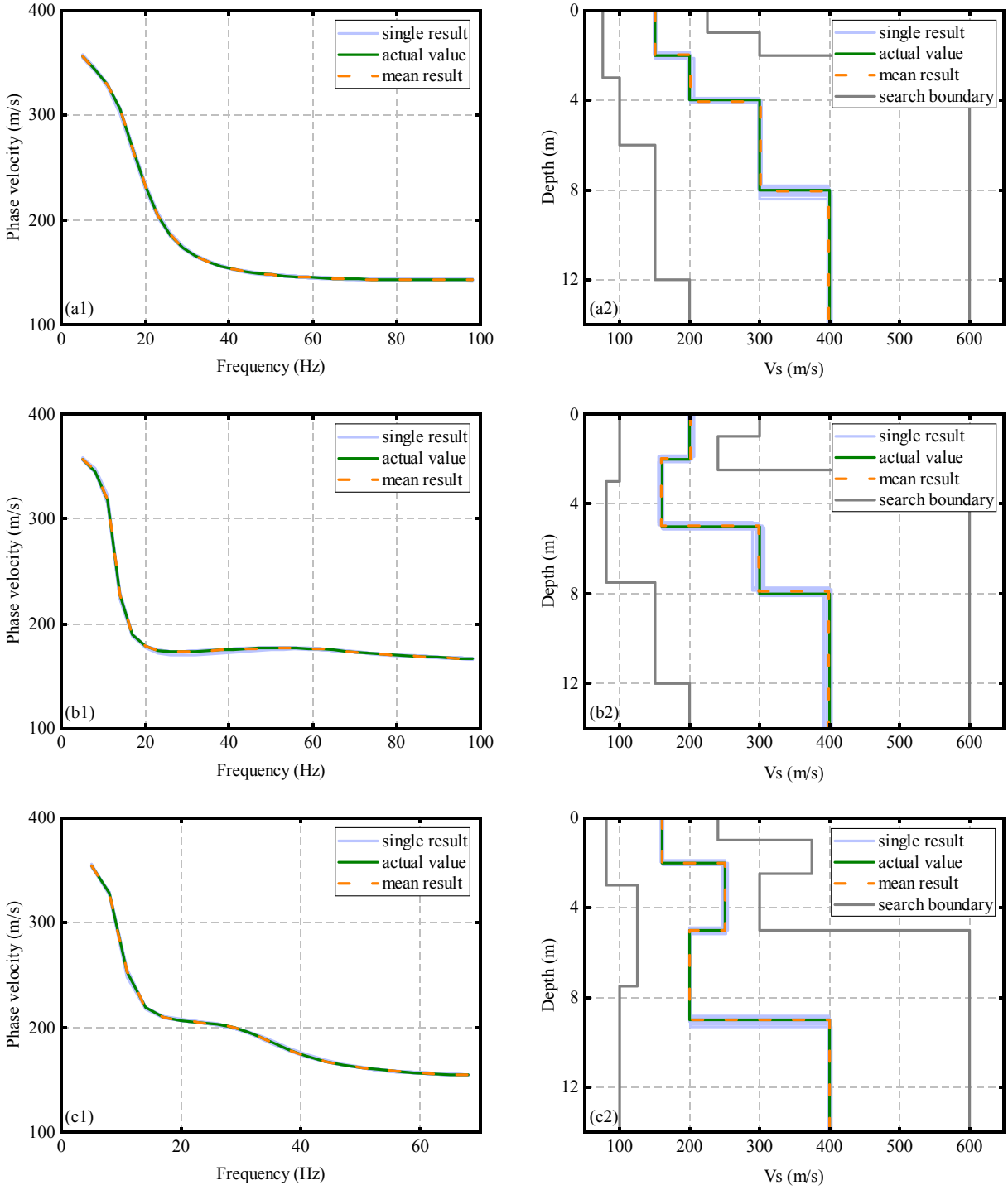

Figure 4. Inversion results of noise-free data of models A, B, and C. Dispersion curves (a1, b1, c1); Shear wave velocity structures (a2, b2, c2).

3.2 Noise-contaminated model inversion

The three models established above do not contain any noise. However, when seismic data are collected in the field, they are often subject to various interferences, causing the collected seismic data to contain noise signals. Noise-contaminated seismic data can have a certain impact on the extraction of dispersion curves [Zhang, 2003], affecting the accuracy of inversion results. Therefore, to examine and evaluate the impact of noise-contaminated Rayleigh wave data on IWOA performance, random noise with an amplitude based on 10% of the phase velocity mean value as perturbations was added to the above models A, B, and C. Then, IWOA was applied to invert the dispersion curves on the three models. The inversion results can be found in Figure 5 and Table 4. The noise addition formula is as follows:

$$v_d = v + d \times \frac{\sum_{i=1}^{N} v_i}{N} \times (rand - rand) \tag{19}$$

Where v_d represents the dispersion curve data after adding noise; v represents the original dispersion curve data, N represents the number of dispersion points of the Rayleigh surface wave, $rand$ represents a random number between 0 and 1, and the formula $rand - rand$ is to increase randomness.

Figures a1, b1, and c1 in Figure 5 represent the dispersion curves before and after inversion for models A, B, and C, respectively. The light blue solid lines represent the dispersion curve results for each independent inversion run (a total of 20 runs). The green solid lines represent the theoretical dispersion curves. The orange dashed lines represent the averaged dispersion curve results over the 20 runs. Figures a2, b2, and c2 in Figure 5 show the shear wave velocity structures before and after inversion for models A, B, and C, respectively. The light blue solid lines represent the shear wave velocity results for each independent inversion run (20 runs in total). The green solid lines represent the true shear wave velocity structures. The orange dashed lines represent the averaged shear wave velocity results over the 20 runs. Table 4 provides a statistical summary of the results of IWOA applied to the inversion of dispersion curves for both noise-contaminates and noise-free models A, B, and C. Table 4 includes the mean, relative error, and standard deviation results for each inversion parameter.

From Figure 5, it can be observed that the inversion results for the dispersion curves show a good overall fit with the theoretical dispersion curves after adding noise. The reconstructed shear wave velocity structures after inversion closely match the actual shear wave velocity profiles, especially the best inversion results in model B. According to the results in Table 4, it can be calculated that the average relative errors of models A, B, and C are 3.56%, 1.18%, and 1.26% respectively, and the average standard deviations are 0.99, 1.72, and 0.78 respectively. In summary, compared with the inversion results of the noise-free model, although the average relative error and average standard deviation of the inversion results of the shear wave velocity and layer thickness of the noise-contaminated model have increased overall, the changes are smaller. The final inversion results still exhibit a good fit with the theoretical dispersion curves. Based on the above discussion, it can be seen that IWOA has good noise immunity and can be well applied in the study of noise-contaminated Rayleigh wave dispersion curve inversion.

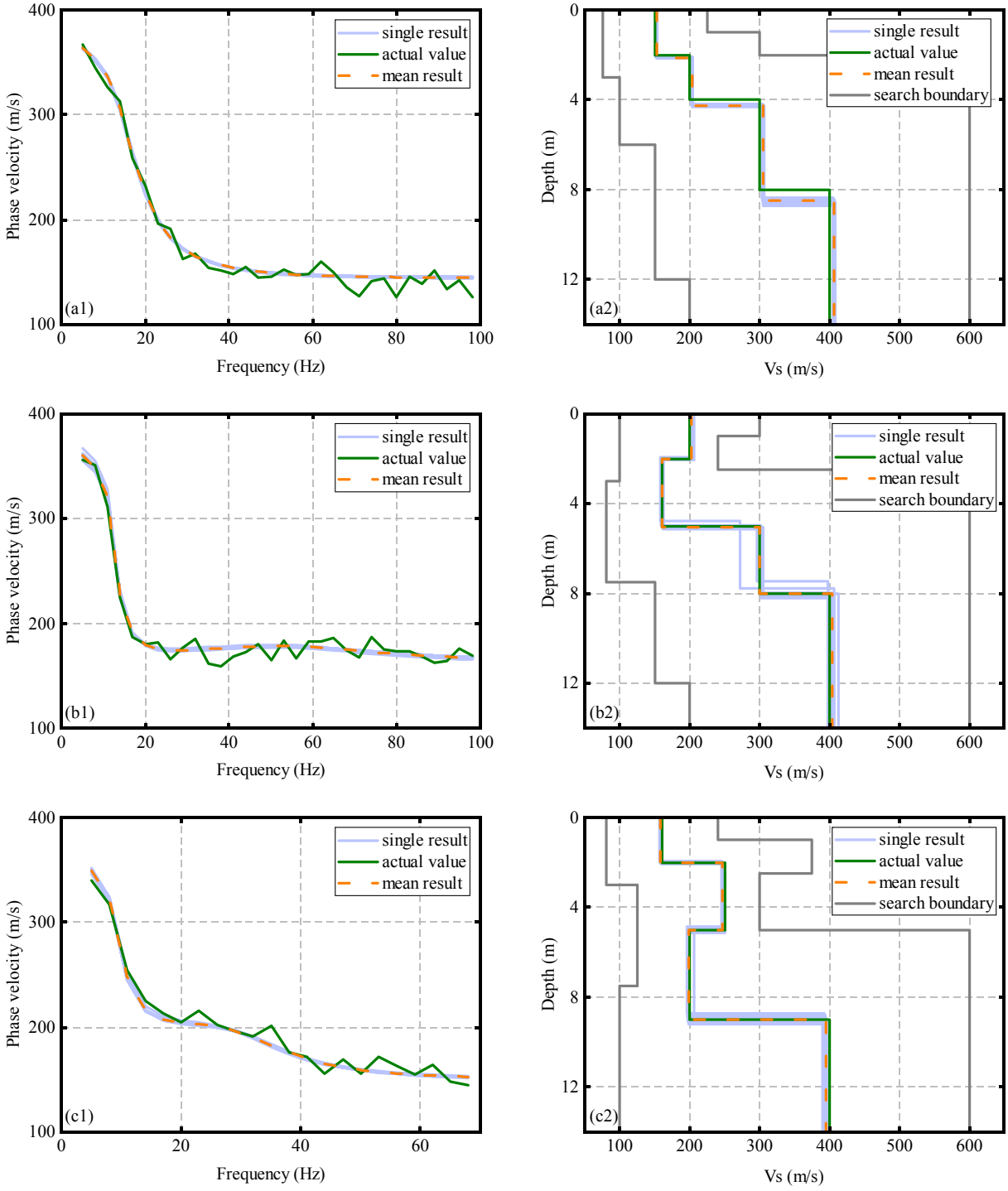

Figure 5. Inversion results of noise-contaminated data of models A, B, and C. Dispersion curves (a1, b1, c1); Shear wave velocity structures (a2, b2, c2).

Model	Inversion parameters	True value	Noise-free data			Noise-contaminated data		
			Inversion mean	Relative error/%	Standard deviation	Inversion mean	Relative error/%	Standard deviation
A	V_{S1}	150	150.03	0.26	0.49	152.43	1.62	0.34
	V_{S2}	200	200.36	0.41	1.57	203.25	1.62	0.45
	V_{S3}	300	300.06	0.27	1.01	304.87	1.62	0.9
	V_{S4}	400	400.05	0.26	1.3	406.49	1.62	5.11
	H_1	2	2	1.19	0.03	2.12	6.02	0.02
	H_2	2	2.01	1.26	0.03	2.12	6.09	0.02
	H_3	4	4.02	1.34	0.08	4.25	6.34	0.06
B	V_{S1}	200	200.33	0.47	1.75	201.99	1	1.33
	V_{S2}	160	159.46	0.65	1.63	160.75	0.67	0.89
	V_{S3}	300	299.09	1.1	4.46	300.38	1.18	6.81
	V_{S4}	400	399.12	0.45	2.78	403.89	1.04	2.81
	H_1	2	1.98	2.33	0.06	2.02	1.25	0.03
	H_2	3	2.99	1.53	0.07	3.01	1.27	0.05
	H_3	3	2.93	2.66	0.16	2.99	1.86	0.14
C	V_{S1}	160	159.98	0.18	0.43	158.09	1.2	0.54
	V_{S2}	250	249.97	0.18	0.67	247.21	1.12	1.13
	V_{S3}	200	199.98	0.18	0.54	198	1.29	1.93
	V_{S4}	400	399.95	0.18	1.07	394.93	1.27	1.7
	H_1	2	2	0.97	0.03	2	1.27	0.03
	H_2	3	3	0.94	0.04	2.99	1.36	0.05
	H_3	4	4.01	1.07	0.06	4	1.31	0.07

Table 4. Statistical table of inversion results of models A, B, and C with and without noise.

3.3 Multi-mode data inversion

In some simple geological models, the dispersion curve of the Rayleigh waves is typically dominated by the fundamental-mode waves. However, when the geological models contain complex models such as low-velocity layers, higher-mode waves may develop in the high-frequency portion of the dispersion curve. At this time, joint inversion of the dispersion curves of multiple modes can improve the accuracy of the inversion results. Therefore, to demonstrate whether IWOA can adapt to multi-mode dispersion curve inversion and improve the accuracy of the inversion results, model B containing a low-speed interlayer was adopted as an example in this paper. High-mode mode data was added to the fundamental-mode wave data of its original model B, and then IWOA was used to invert the noise-free and noise-contaminated data containing multi-mode data. The inversion results are shown in Figure 6, and the error analysis is presented in Table 5. The algorithm's parameter settings remain consistent with those described in Section 3.1.

In Figure 6, it can be seen that whether it is a noise-free model or a noise-contaminated model, the dispersion curve obtained by the inversion model and the multi-mode theoretical dispersion curve fit well (Figure 6a1 and 6b1), and the true values of each model parameter can be well inverted and reconstructed (Figure 6a2 and 6b2). This paper calculated and compared the inversion results for fundamental-mode data (Table 4, model B) only and multi-mode data (Table 5). It was found that the average relative error (with 10% noise) decreased from 1.18% to 1.03%, and the average standard deviation decreased from 1.72 to 1.41 when using multi-mode data for inversion. Based on the above results, it can be verified that using multi-mode data for inversion can indeed reduce the multi-solution nature of the inversion and improve the accuracy of the inversion. It also can be indicated that IWOA is not only suitable for fundamental-mode dispersion curve inversion but can also be applied effectively to the inversion of multi-mode dispersion curves.

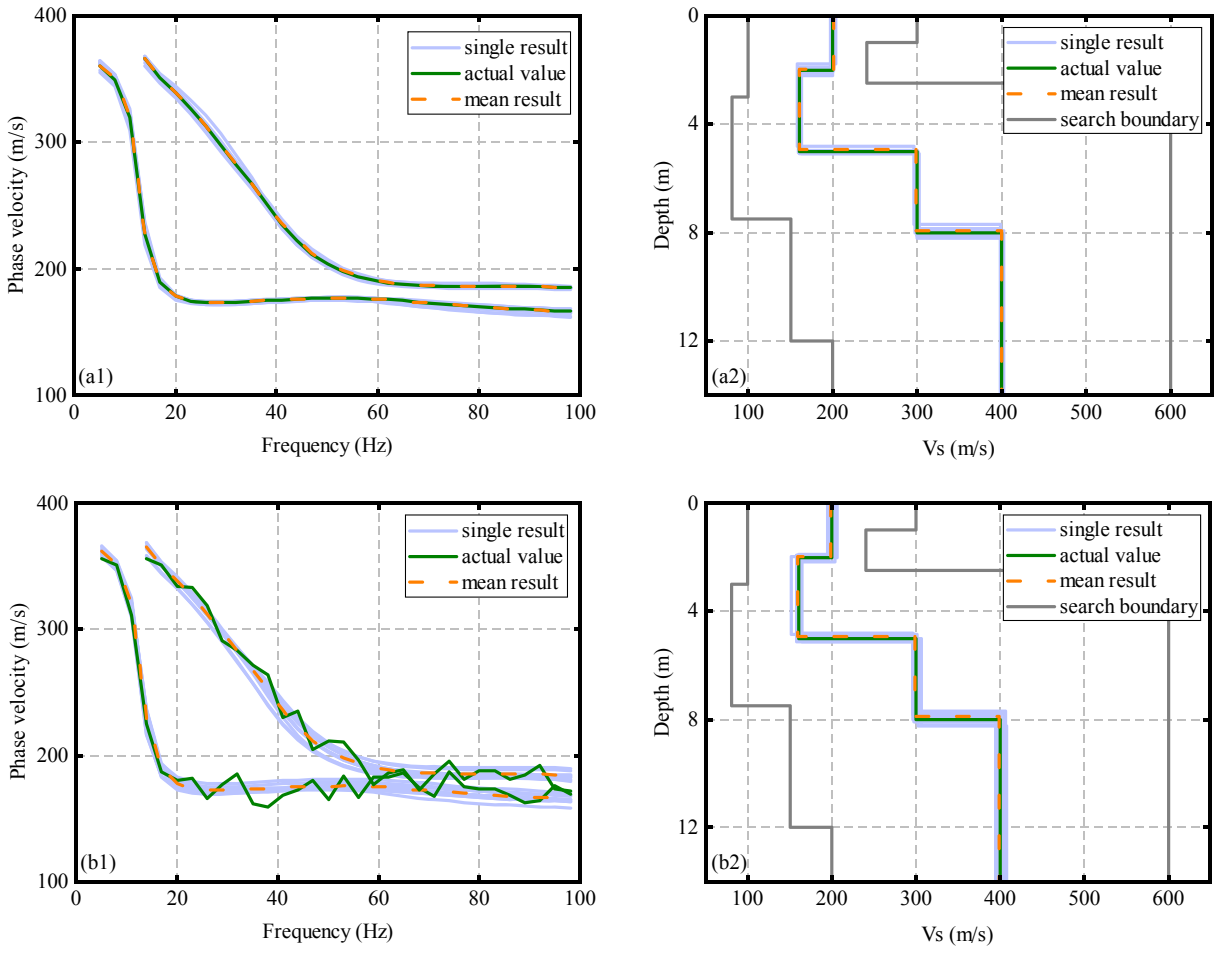

Figure 6. Multi-mode data of model B inversion results without noise (top) and with noise (bottom). Dispersion curves (a1, b1); Shear wave velocity structures (a2, b2).

Inversion parameters	True value	Noise-free data			Noise-contaminated data		
		Inversion means	Relative error/%	Standard deviation	Inversion means	Relative error/%	Standard deviation
V_{S1}	200	201.2	0.67	3.98	198.98	1.05	2.27
V_{S2}	160	159.97	0.18	0.57	159.07	1.13	1.61
V_{S3}	300	300.08	0.13	0.56	298.12	1.1	3.09
V_{S4}	400	400.12	0.13	0.7	399.15	0.78	2.68
H_1	2	1.96	2.9	0.18	1.97	1.15	0.06
H_2	3	2.99	1.54	0.11	2.96	1.01	0.09
H_3	3	3	0.97	0.06	2.97	0.97	0.1

Table 5. Statistical table of inversion results of model B multi-mode data.

3.4 Comparative analysis of algorithms

To verify that IWOA has a stronger search ability than other algorithms, IWOA, WOA, and PSO were used to invert the dispersion curves of model A with and without noise in this paper. To maintain consistency, in terms of algorithm parameter settings, the population number of the three algorithms was set to 20, the number of iterations was set to 100, and the number of inversions was set to 10. The convergence curves of the three algorithms (the average of 10 convergence curves) are shown in Figure 7. The shear wave velocity results (the average of 10 inversion results) inverted by the three algorithms are shown in Figure 8. Table 6 shows the parameters of the inversion of the three algorithms, namely the minimum fitness value, inversion time, and relative error (all are the average results of 10 inversions).

It can be observed from Figure 7a (noise-free model) that in the process of 100 iterations, PSO (orange) is in the convergence state after about the 10^{th} iteration, WOA (red) enters the convergence state around the 40^{th} iteration but converges process is unstable, and the IWOA (blue) reaches convergence at iteration 93. In Figure 7b (noise-contaminated model), it can be observed that in the process of 100 iterations, PSO (orange) almost converges after the 60^{th} iteration, WOA (red) enters the convergence state after about the 20^{th} iteration, and IWOA (blue) shows convergence around the 80^{th} iteration. As can be seen from Table 6, although IWOA requires more iterations and time to reach the convergence state, the convergence process of IWOA is the most stable and the final fitness value is also the smallest. It can also be seen in Figure 8 that the shear wave velocity results of IWOA inversion are closest to the real model among the inversion results of the three algorithms. In general, compared with WOA and PSO, IWOA has the best performance in the inversion of the two models. At the same time, it also proves that this algorithm has strong competitiveness and broad development space in the field of dispersion curve inversion.

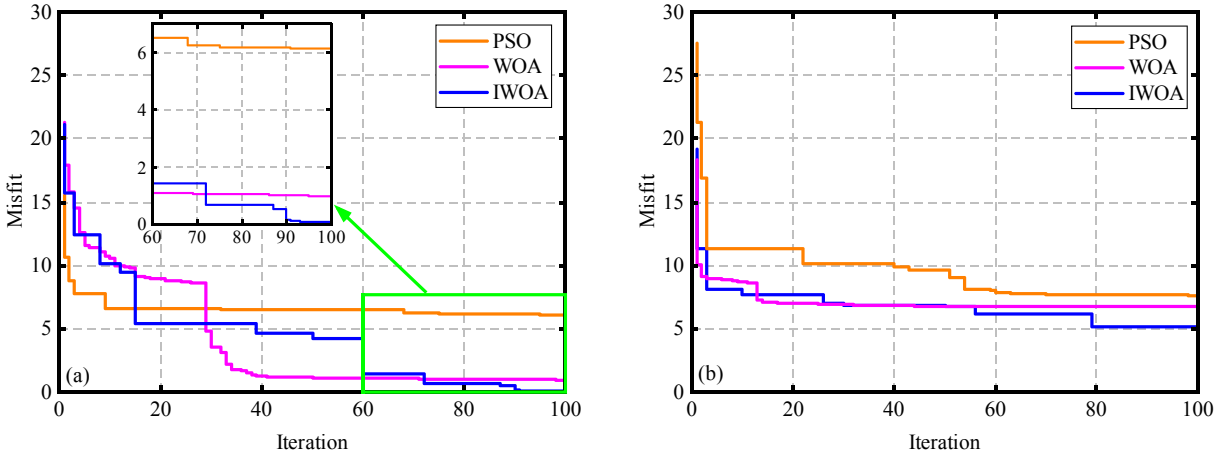

Figure 7. The convergence processes of the algorithm in model A without noise (a) and with noise (b).

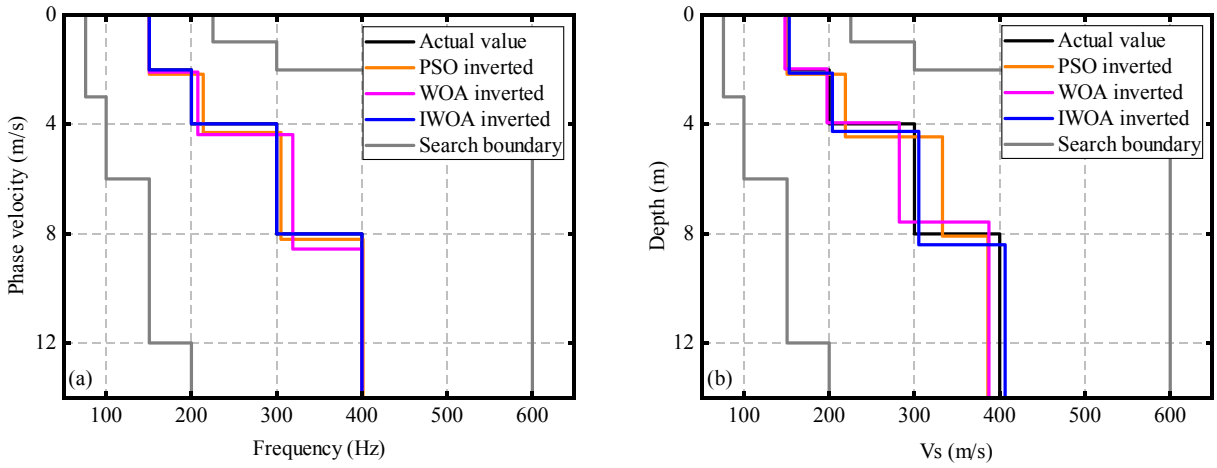

Figure 8. Inversion results of shear wave velocity structures in model A without noise (a) and with noise (b).

Algorithms	Noise-free data			Noise-contaminated data		
	Minimum fitness value	Inversion time/s	Relative error/%	Minimum fitness value	Inversion time/s	Relative error/%
PSO	6.13	315	3.67	7.63	320	7.9
WOA	0.96	712	4.74	6.73	756	3.39
IWOA	0.53	727	0.08	5.12	807	3.27

Table 6. Statistical table of inversion results of model A data.

4. Measured data inversion analysis

To further verify the inversion ability of IWOA applied to measured seismic data, this paper selected measured data from two regions and inverted the fundamental-mode and multi-mode dispersion curves respectively.

4.1 Data A

Data A is the measured surface wave data collected at the A2 test point around Arnarbæli on the Ölfusá River in southern Iceland. The geographical location of the Arnarbæli study area is shown in Figure 9. Regarding the collection of seismic records, 24 geophones with a main frequency of 4.5 Hz, a channel spacing of 1 m, a gun detection distance of 10 m, a hammered source for the source, and a sampling frequency of 1000 Hz [Olafsdottir, 2016]. Figure 10a displays the collected seismic records, and Figure 10b shows the dispersion energy map extracted from the collected seismic records. It can be seen from Figure 10b that the fundamental-mode dispersion curve is well developed, so the fundamental-mode data of the measured data was selected for inversion in this paper. The various inversion parameter settings are the same as the theoretical model test. Refer to the parameter settings in [Olafsdottir, 2016; Chen et al. 2023]] to set the geological parameters of each layer and the model search range. The geological model parameters and search scope for the inversion are shown in Table 7.

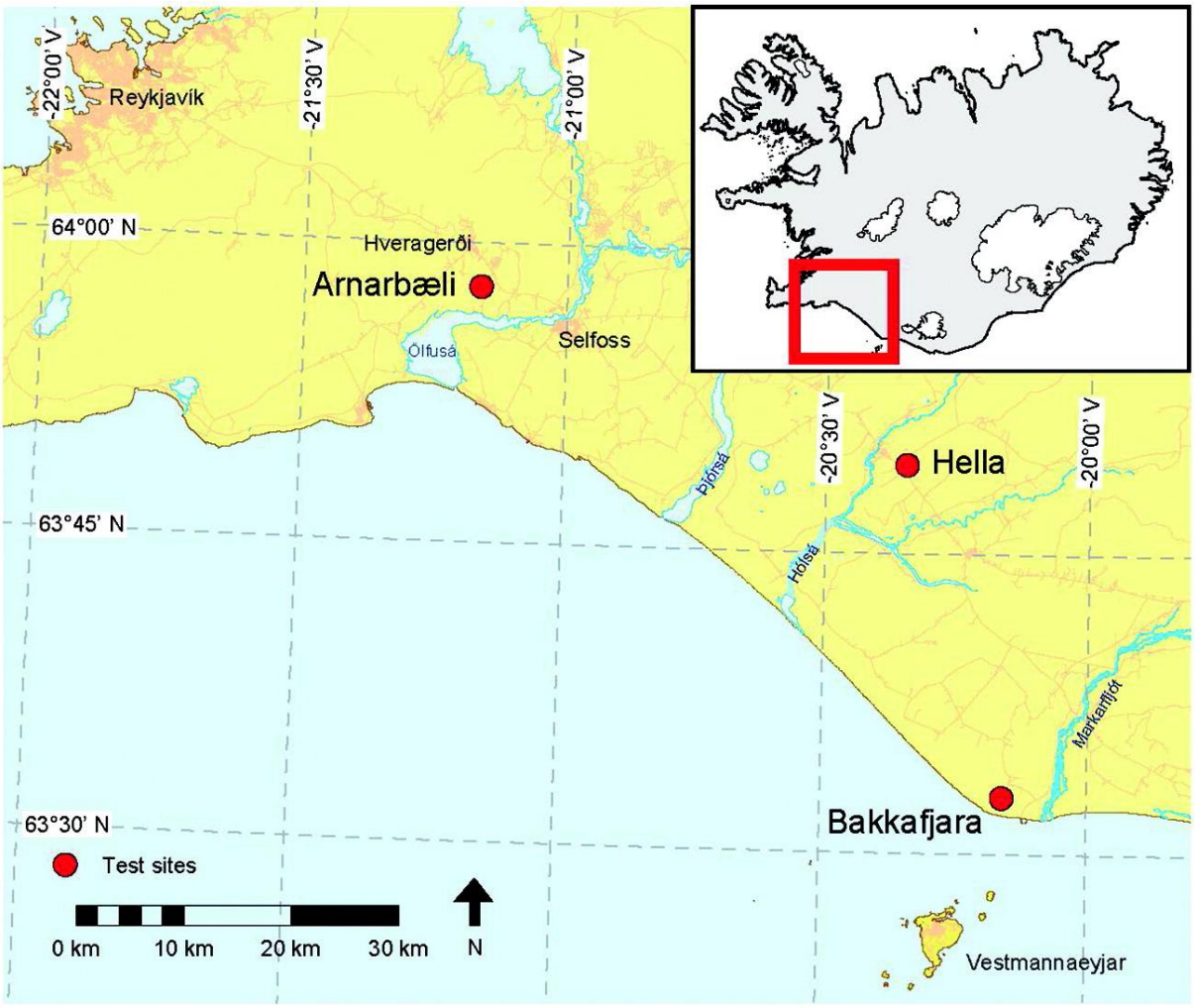

Figure 9. Geographical location of the Arnarbæli study area.

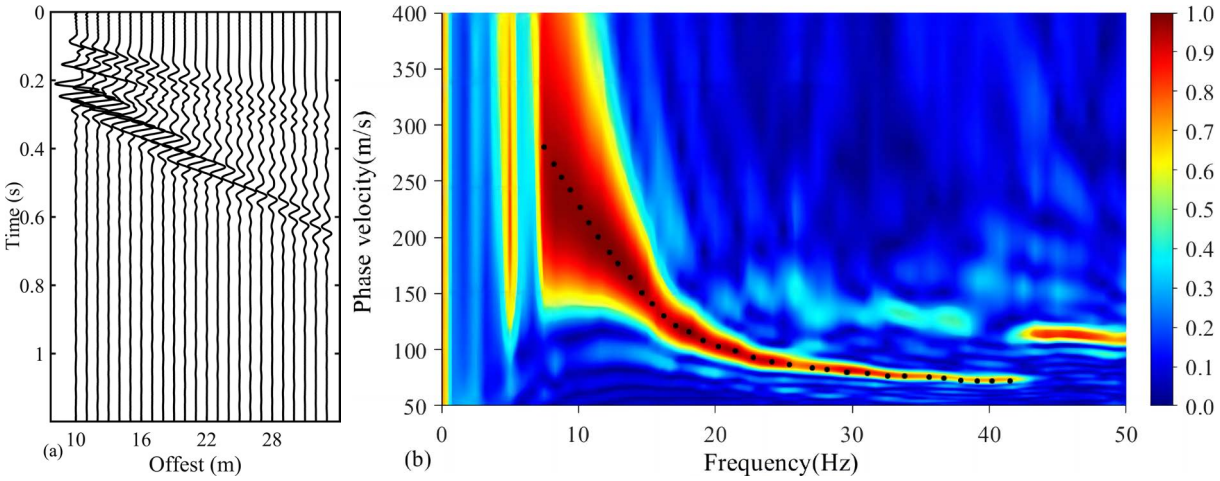

Figure 10. Measured seismic data (a) and dispersion energy map (b).

Layer number	Geological parameters				Search scope	
	H [m]	V_S [m/s]	V_P [m/s]	ρ [g/cm^3]	V_S [m/s]	H [m]
1	0.8	78	1440	1.85	60~90	0.2~1.2
2	0.5	80	1440	1.85	70~100	0.2~1.2
3	0.7	92	1440	1.85	80~110	0.2~1.2
4	1.2	111	1440	1.85	90~130	0.4~2
5	1.9	141	1440	1.85	100~180	0.4~2
6	3	184	1440	1.85	130~240	1.8~4
7	4.7	230	1440	1.85	180~280	3~5.5
8	7.5	277	1440	1.85	230~330	5.8~9
9	5.2	350	1440	1.85	300~400	4~6
10	∞	350	1440	1.85	300~400	∞

Table 7. Estimated geological parameters and model parameters search range [Olafsdottir, 2016; Chen et al. 2023].

The inversion results are shown in Figure 11. Figure 11a shows the comparison between the dispersion curve obtained from the IWOA inversion (red line) and the real dispersion curve (black dots). It can be seen from Figure 11a that the real dispersion curve fits the dispersion curve obtained by the inversion very well. Figure 11b shows the change in the objective function value during the iterations for the IWOA inversion. It can be seen from Figure 11b that IWOA reaches the convergence state around the 90th iteration, and the final fitness value is relatively low.

Figure 11c shows the shear wave velocity structures of the IWOA inversion result(red line), the real velocity structure[Olafsdottir, 2016] (orange line), and the velocity structure resulting from the hybrid particle swarm optimization algorithm (HPSO) [Chen et al., 2023] (blue line). It can be seen from Figure 11c that there is a certain deviation between the shear wave velocity structure inverted by IWOA and the actual shear wave velocity structure, but the overall consistency is high. Compared with the inversion results of HPSO, the shear wave velocity structure inverted by IWOA is closer to the real shear wave velocity structure, especially in the shallow area of 0-12 meters. While in the deeper subsurface layers, the inversion result of IWOA is slightly worse than those of HPSO. Based on the above analysis, it can be concluded that IWOA is effective in inverting Rayleigh wave dispersion curves from measured data, and the inversion results in shallow layers are more credible.

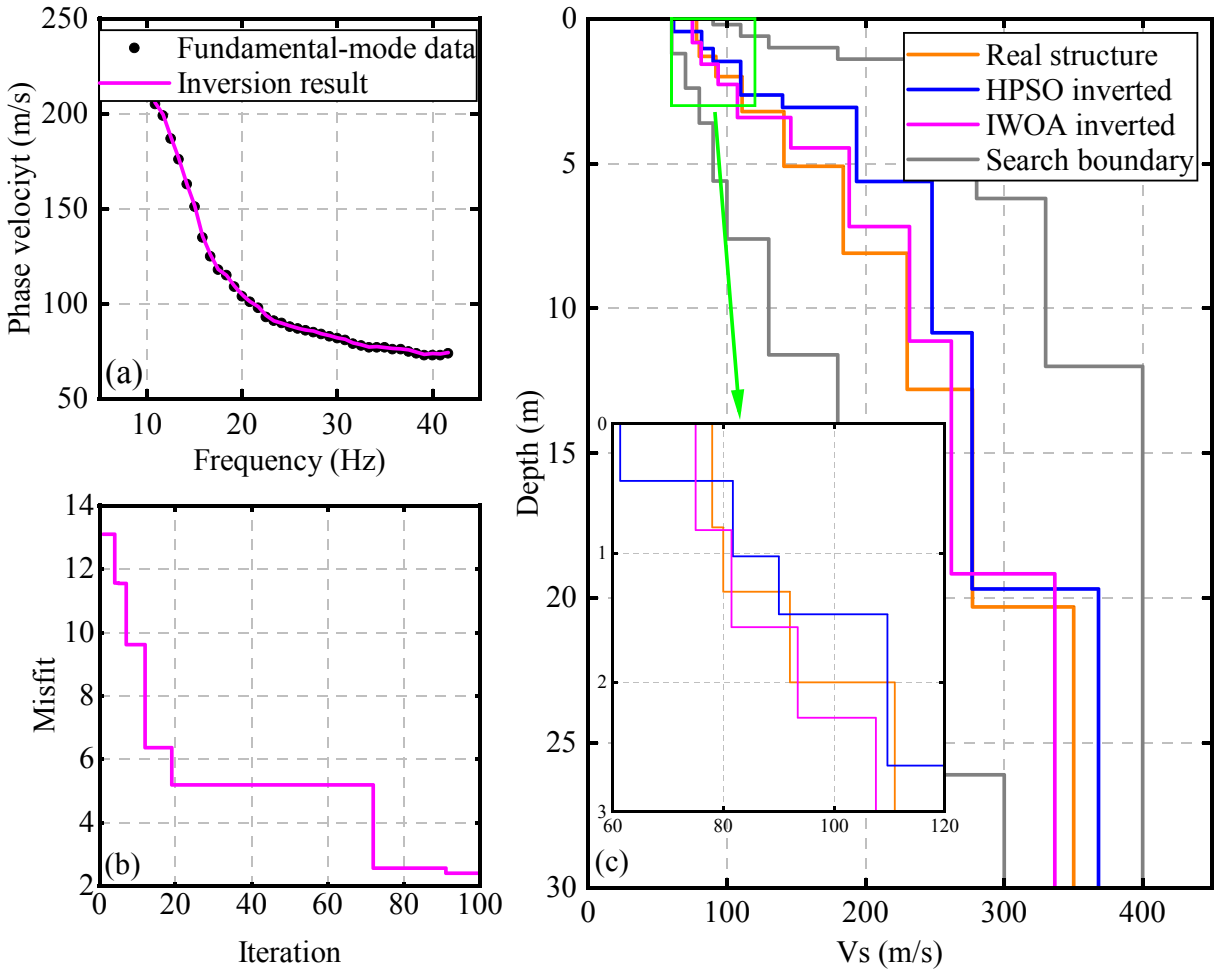

Figure 11. The measured data A inversion results. Dispersion curve results (a); Convergence processes (b); Shear wave velocity results (c).

4.2 Data B

Data B is the measured seismic surface wave data in the Wyoming area of the United States [Xia et al., 2002]. Regarding the collection of seismic records, 48 vertical component geophones with a main frequency of 8 Hz, a 6.3 kg hammer source, a channel spacing of 0.9 m, and a minimum offset of 0.9 m. Figure 12a displays the collected seismic records [Xia et al., 2002], and Figure 12b shows the dispersion energy map extracted from the collected seismic records [Xia, 2002]. It can be seen from Figure 12b that there are multi-mode dispersion curves (black dots). According to Section 3.3 of the article, it can be seen that multi-mode dispersion curves can improve the accuracy of inversion. Therefore, this article chooses to use multi-mode dispersion curve data for joint inversion to ensure that

high-precision inversion results can be obtained. The various parameter settings of the inversion are the same as those of the theoretical model test. According to the lithology division and shear wave velocity in the well logging data in the study area, the underground medium can be roughly divided into five layers. The estimated Poisson's ratio and density values for each layer, as well as the search range for shear wave velocity and layer thickness [Cai et al., 2018] are shown in Table 8.

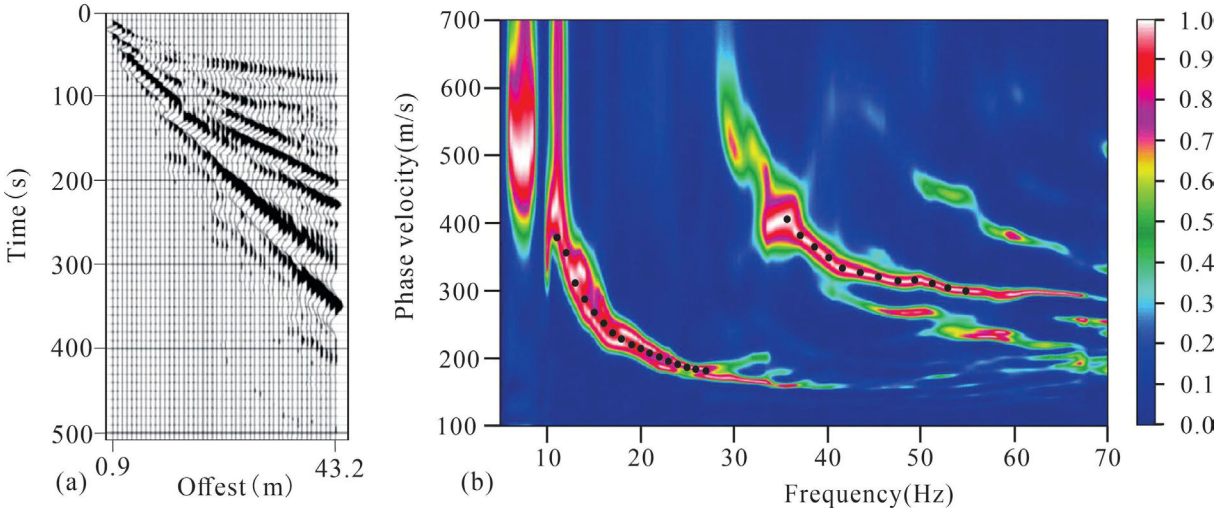

Figure 12. Measured seismic data (a) and dispersion energy map (b).

Layer number	Geological parameters		Search scope	
	Poisson's ratio	ρ [g/cm^3]	V_S [m/s]	H [m]
1	0.38	2	100~300	1~5
2	0.38	2	100~400	1~5
3	0.35	2	100~600	1~5
4	0.35	2	200~600	1~5
5	0.30	2	200~800	∞

Table 8. Estimated geological parameters and model parameters search range [Cai et al., 2018].

The inversion results are shown in Figure 13. Figure 13a is a comparison diagram between the dispersion curve (red line) obtained by IWOA inversion and the actual dispersion curve (black dots). As can be seen from Figure 13a, the real dispersion curves of the fundamental-mode and high-mode are in good agreement with the dispersion curve inversion results. Figure 13b shows the change in the objective function value during the iterations for the IWOA inversion. As can be seen from Figure 13b, IWOA reaches the convergence state at the 55th iteration, and the entire convergence process is relatively stable. Figure 13c shows the shear wave velocity structures of the IWOA inversion result(red line), the velocity structure logging data [Xia et al., 2002] (orange solid line with black diamonds), and Xia's inversion results [Xia, 2014] through a local linear optimization algorithm (blue solid line with

black dots). It can be seen from Figure 13c that the IWOA inversion results and the logging data fit well. Compared with Xia's inversion results, IOWA's inversion results are better in the range of 5~12m in the middle stratum. Based on the above analysis, it can be concluded that for measured surface wave data containing multi-mode dispersion curves, the inversion of IWOA can still achieve good results, which can solve practical work and problems effectively.

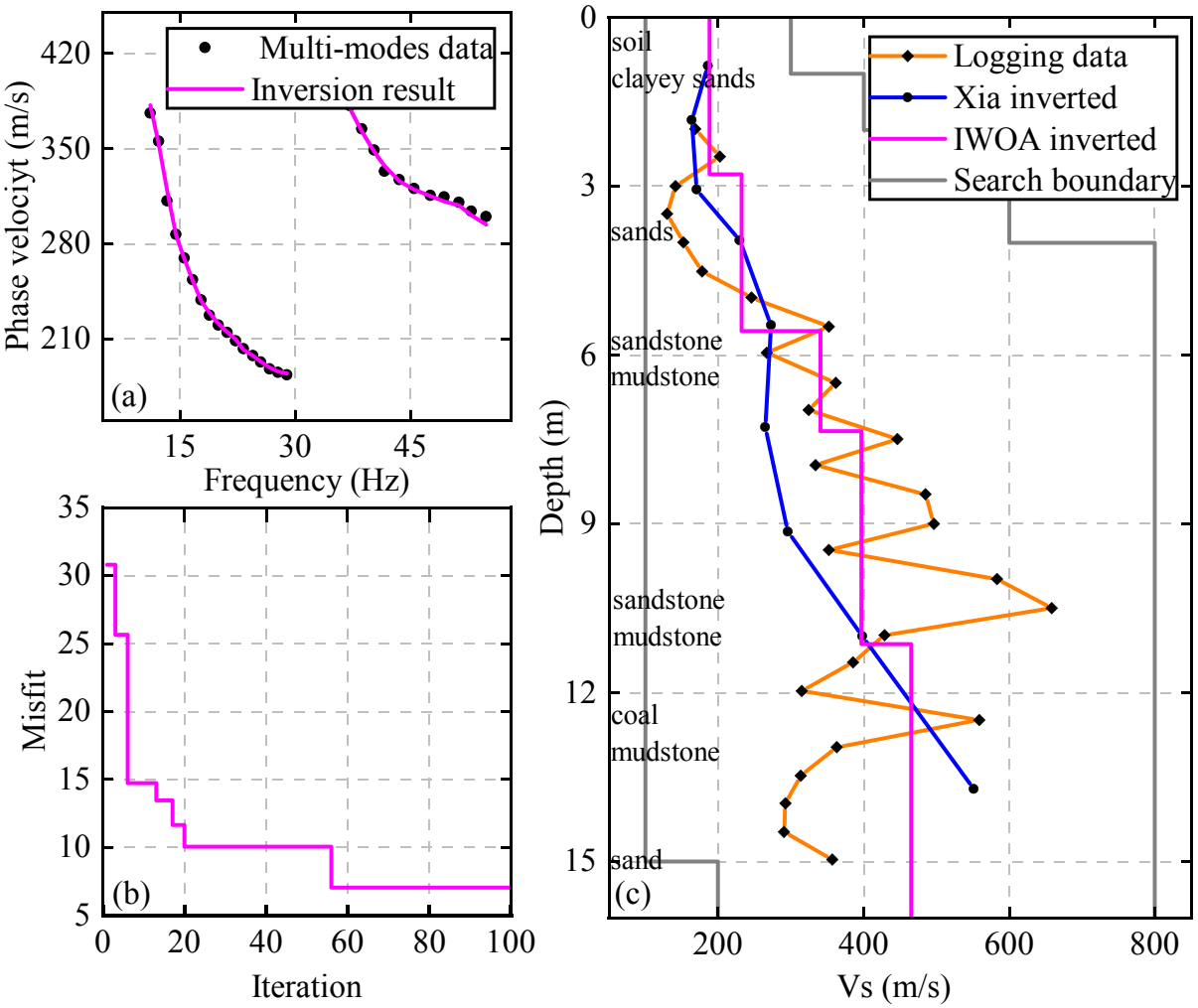

Figure 13. The measured data A inversion results. Dispersion curve results (a); Convergence processes (b); Shear wave velocity results (c).

5. Conclusion

This paper introduces the IWOA in the study of the Rayleigh wave dispersion curve inversion by improving the traditional WOA from two aspects: population initialization and adaptive weight coefficient. Firstly, two complex multimodal functions are used to test the optimization ability of the algorithm. Secondly, IWOA is applied to the inversion analysis of the fundamental-mode and multi-mode Rayleigh wave dispersion curves of the theoretical model with and without noise. Then, the IWOA, PSO, and WOA were used for comparative analysis experiments. Finally, IWOA was applied in the dispersion curve inversion analysis of the measured data. The following conclusions were drawn:

1) In the optimization test of two complex multimodal functions, the results show that IWOA can converge well to the theoretical solution. Compared with traditional WOA, the capabilities of global search and jumping out of local optimal solutions of IWOA are significantly improved.

2) In the dispersion curve inversion of three theoretical models with noise and without noise, IWOA can get higher-precision inversion results and the inversion results are very close to the theoretical models, which proves that IWOA has the advantages of high applicability and good noise resistance. At the same time, IOWA can also be applied to the inversion of the dispersion curve of multi-mode Rayleigh surface waves to improve the accuracy of inversion results. Compared with PSO and WOA, IWOA has higher convergence accuracy and a more stable convergence process. In summary, the IWOA has a good development potential and broad development space in the field of surface wave dispersion curve inversion in the future.
3) In the dispersion curve inversion of measured data, the velocity structure obtained by IWOA inversion is basically consistent with the real data, especially in shallow strata, which have better inversion results. The dispersion curve is highly consistent with the real dispersion curve, which also verifies the practicability of IWOA. Regarding the relatively less favorable results in deep subsurface inversion, my next step is to consider integrating the IWOA with other global nonlinear algorithms to jointly invert the dispersion curve to improve the accuracy of the inversion results of deep strata.
4) Measured data analysis shows that whether it is the global optimization algorithm or the IWOA algorithm used in this article when the dispersion curve is fully fitted, the inversion results are still not highly consistent with the real model, and there are certain errors. This is mainly due to multiple interpretations of inversion. Therefore, in addition to studying the algorithm itself, more prior information should be integrated into the objective function and constrained based on extracting multi-mode dispersion curves and reducing the solution space in actual data processing to reduce the multiple solutions of the inversion.

Funding. This work was supported by the National Natural Science Foundation of China Youth Project [42004113], Jiangxi Provincial Natural Science Foundation Project [20212BAB211003, 20224BAB213049], National Science and Technology Supporting Program of Jiangxi Province [20232BAB213079], China National Nuclear Corporation-State Key Laboratory of Nuclear Resources and Environment (East China University of Technology) Joint Innovation Fund Project [2023NRE-LH-08] and Jiangxi University Students Innovation and Entrepreneurship Project [S202310405011, S202310405036].

References

Beaty, K., D. Schmitt and M. Sacchi (2002). Simulated annealing inversion of multimode Rayleigh wave dispersion curves for geological structure, Geophys. J. Int., 151, 2, 622-631.

Bui, D., M. Abdullahi, S. Ghareh, H. Moayedi and H. Nguyen (2021). Fine-tuning of neural computing using whale optimization algorithm for predicting compressive strength of concrete, Engin. with Compu., 37, 1, 701-712.

Cai, W., X. Song, S. Yuan and Y. Hu (2018). Fast and stable Rayleigh wave dispersion curve inversion based on particle swarm optimization, Oil Geophys. Prosp., 53, 1, 25-34.

Calderon, C. and B. Luke (2007). Improved parameterization to invert Rayleigh-wave data for shallow profiles containing stiff inclusions, Geophysics, 72, 1, 1-10.

Cercato, M. (2010). Addressing non-uniqueness in linearized multichannel surface wave inversion, Geophys. Prosp., 57, 1, 27-47.

Chen, H., H. Li, T. Li, H. Ai, J. Zhang and T. Dai (2023). Inversion of Rayleigh surface wave dispersion curve by hybrid particle swarm optimization algorithm, Oil Geophys. Prosp., 58, 3, 598-609.

Constable, S., R. Parker and C. Constable (1987). Occam's inversion: A practical algorithm for generating smooth models from electromagnetic sounding data, Geophysics, 52, 3, 267-462.

Ding, H. (2004). A fast and reliable method for inversion of Rayleigh wave dispersion curves based on SVD algorithm, Chinese Journal of Engineering Geophysics, 4, 304-308.

Dorman, J. and M. Ewing (1962). Numerical inversion of seismic surface wave dispersion data and crust-mantle structure in the New York Pennsylvania area, Journal of Geophysical Research, 67, 13, 5227-5241.

Fan, Y., J. Liu and B. Xiao (2002). Fast vector-transfer algorithm for computation of Rayleigh wave dispersion curves, Journal of Hunan University, 5, 25-30.

Lei, Y., H. Shen, X. Li, X. Wang and Q. Li (2019). Inversion of Rayleigh wave dispersion curves via adaptive GA and nested DLS, Geophys. J. Int., 1, 547-559.

Mirjalili, S. and A. Lewis (2016). The whale optimization algorithm, Adv. Engin. Softw., 95, 51-67.
Ni, R., H. Li, Q. Xie, F. Guan, G. Huang, J. Zhang and H. Zhang (2018). Acoustic inversion method for parameters of seafloor sediment based on Gassmann theory and genetic algorithm, Sci.Tech. Engin., 18, 6, 223-228.
Olafsdottir, E. (2016). Multichannel analysis of surface waves for assessing soil stiffness, Faculty of Civil and Environmental Engineering University of Iceland, Reykjavik, Iceland, 104-108.
Rayleigh, L. (1885). On waves propagated along the plane surface of an elastic solid, Proceedings of the London Mathematical Society, s1-17, 1, 4-11.
Ryden, N. and C. Park (2006). Fast simulated annealing inversion of surface waves on pavement using phase-velocity spectra, Geophysics., 71, 4, 49-58.
Shi, Y. and W. Jin (1995). Genetic algorithms inversion of lithospheric structure from surface wave dispersion, Chinese J. Geophys., 38, 2, 189-198, (in Chinese)
Song, X., L. Tang, X. Lv, H. Fang and H. Gu (2012). Application of particle swarm optimization to interpret Rayleigh wave dispersion curves, J. Appl. Geophys., 84, 9, 1-13.
Sun, X., Z. Ji and Q. Yang (2022). Inversion of Rayleigh wave dispersion curves based on the improved sparrow search algorithm, Geophysical and Geochemical Exploration, 46, 5, 1267-1275.
Wang, Y. and H. Gu (2009). Research on multi-mode surface wave joint inversion using OCCAM algorithm, Yellow River., 31, 3, 92-94.
Wu, D., C. Sun and M. Lin (2017). Active seismic surface wave dispersion imaging method based on cross-correlation and phase-shifting, Progress Geophys., 32, 4, 1693-1700.
Xu, M. and J. Wu (2014). Application of multi-channel transient Rayleigh wave in geological exploration, Appl. Mech. Mat., 638-640.
Xia, J. (2014). Estimation of near-surface shear-wave velocities and quality factors using multichannel analysis of surface-wave methods, J. Appl. Geophys., 103, 140-151.
Xia, J., R. Miller, C. Park, E. Wightman and R. Nigbor (2002). A pitfall in shallow shear-wave refraction surveying, J. Appl. Geophys., 51, 1, 1-9.
Yang, D. and J.E. (2009). An adaptive chaos immune optimization algorithm with mutative scale and its application, Control Theory and Technology, 26, 10, 1069-1074.
Zhang, J. and J. Wang (2020). Improved whale optimization algorithm based on nonlinear adaptive weight and golden sine operator, Intelligent Compu. Applic., 10, 9, 43-48.
Zhang, Z. (2003). Application of Rayleigh surface wave exploration in cavity detection, Hunan Hydro Power., 1, 19-20.
Zhang, W. (2018). Application of integrated geophysical exploration in geological disaster exploration, West-China Expl. Engin., 30, 9, 195-161.
Zhang, X., W. Du and Y. Lu (2016). The application of particle swarm optimization in the inversion of Rayleigh wave dispersion curve, Journal of Liaoning Technical University (Natural Science), 35, 12, 1527-1532.
Zhang, X., N. Ma, W. Fu, W. Ji, S. Zhang and Y. Diao (2023). Adaptive whale optimization algorithm based on chaotic mapping and quadratic interpolation, Compu. Engin. Des., 44, 4, 1088-1096.
Zhou, Z., C. Ma and Z. Si (2008). The application and evaluation on the effect of transient state Rayleigh wave exploration technique to the landslide survey, Chinese J. Engin. Geophys., 5, 1, 9-13.
Zhu, Q., W. Zhang, E. Di and Y. Shi (2022). Research on quality evaluation of widening subgrade of land embankment avenue based on Rayleigh wave nondestructive testing technology, BeiFang JiaoTong., 05, 41-45.

***CORRESPONDING AUTHOR: Zhenan YAO**,
East China University of Technology, China
e-mail: an6428060@163.com